A 3D Feature Descriptor Recovered from a Single 2D Palmprint Image

Qian Zheng[1,2], Ajay Kumar[1], and Gang Pan[2]

Abstract—Design and development of efficient and accurate feature descriptors is critical for the success of many computer vision applications. This paper proposes a new feature descriptor, referred to as DoN, for the 2D palmprint matching. The descriptor is extracted for each point on the palmprint. It is based on the ordinal measure which partially describes the difference of the neighboring points' normal vectors. DoN has at least two advantages: 1) it describes the 3D information, which is expected to be highly stable under commonly occurring illumination variations during contactless imaging; 2) the size of DoN for each point is only one bit, which is computationally simple to extract, easy to match, and efficient to storage. We show that such 3D information can be extracted from a single 2D palmprint image. The analysis for the effectiveness of ordinal measure for palmprint matching is also provided. Four publicly available 2D palmprint databases are used to evaluate the effectiveness of DoN, both for identification and the verification. Our method on all these databases achieves the state-of-the-art performance.

1 Introduction

Automated personal identification using biometrics characteristics is one of the most critical and challenging tasks to meet growing demand for stringent security. There is ever growing need to develop more accurate and efficient biometrics matching technologies. Therefore our goal in this work has been to design, develop and evaluate more accurate, compact and faster matching algorithms for the palmprint identification. In the context of advancements in the matching of 2D palmprints, this paper introduces new algorithm to further improve feature extraction and matching techniques for the contactless palmprint identification. Our key contributions are three-folds: 1) we present a new palmprint feature which is efficient and effective for 2D palmprint matching; 2) we show that such feature describes the 3D information and it can be extracted from a single 2D palmprint image; 3) our feature is based on the ordinal measure and we show that the ordinal measure is powerful for palmprint matching. Our method[1] achieves the state-of-the-art performance on four publicly available 2D palmprint databases. Besides, extra experiments are well designed to verify our arguments on contribution 2) and 3).

The paper is organized as follows: we first introduce the DoN feature and explain its recovery from a single 2D image in Sec. 2; the effectiveness of the ordinal measure is ascertained in Sec. 3; finally, the experimental results are reported in Sec. 4.

2 DoN for Palmprint Matching

In this section, the DoN feature is firstly introduced. We then illustrate that how such feature which describes 3D information can be recovered from a single 2D image. Finally, the extraction of DoN from the 2D palmprint image and the feature matching between two palmprint templates are introduced.

2.1 DoN: Difference of Vertex Normal Vectors

For the better description of the feature, we build Cartesian coordinates for each acquired palmprint image, image plane forming x-y plane, with the normal of image surface $\overrightarrow{\mathbf{N}}$ representing z-axis, as shown in Fig. 1.

Each point/pixel $\mathbf{p}_i$ on the image plane is one-to-one corresponding to a vertex $\mathbf{v}_i$ on palmprint surface. Let $\mathbf{n}_i = (x_i, y_i, z_i)$ denote the normal vector of vertex $\mathbf{v}_i$. Suppose point $\mathbf{p}_i$ has two neighboring regions R_i^1 and R_i^2, its DoN feature $DoN(i)$ is

$$DoN(i) = \tau(\sum_{j \in R_i^1} z_j - \sum_{j \in R_i^2} z_j), \tag{1}$$

where $\tau(\cdot)$ is the sign function which is defined as

$$\tau(\alpha) = \begin{cases} 0, & \alpha < 0, \\ 1, & \alpha \geq 0. \end{cases} \tag{2}$$

The DoN feature for $\mathbf{p}_i$ describes the difference between the z-component of normal vectors from its two neighboring regions. According to (1), two key issues in recovering the DoN feature of point $\mathbf{p}_i$ are: 1) how to obtain z value for each point from its neighboring regions (Sec. 2.2); 2) how to identify the neighboring regions of point $\mathbf{p}_i$ (Sec. 2.3).

2.2 3D Feature from a Single 2D Image

We address the first problem by introducing the Lambertian Model in our analysis. The Lambertian Model has also been utilized by Basri and Jacobs [2] to prove that the Lambertian objects appear close to a 9D linear subspace. This conclusion was evaluated for face recognition problem and excellent performance was achieved [2]. In this paper, we further explore Lambertian Model for the contactless palmprint matching.

[1]*Department of Computing, The Hong Kong Polytechnic University, Hung Hom, Kowloon, Hong Kong;*
[2]*Department of Computer Science, Zhejiang University, Hangzhou, China.*

1. The implementation of proposed method is publicly made available [1]

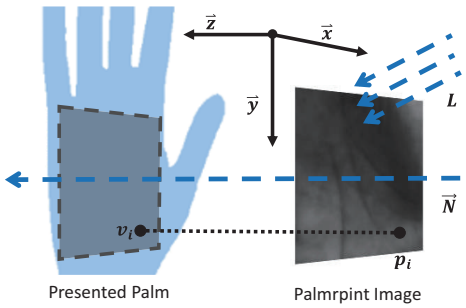

Fig. 1: The 2D palmprint image is essentially the projection of the palmprint surface. The direction of illumination $\mathbf{L}$ is always from the front side of the palmprint imaging.

According to the Lambertian Model, the pixel value $I(i)$ of point $\mathbf{p}_i$ on image I is jointly determined by reflectance k_d, illumination intensity l_d, illumination direction vector $\mathbf{L}$, and point normal vector $\mathbf{n}_i$,

$$I(i) = k_d l_d \mathbf{L}\mathbf{n}_i. \tag{3}$$

For different points on the same palmprint image, k_d, l_d, and $\mathbf{L}$ can be considered as the same.

Given a point $\mathbf{p}_i$, the difference between the points intensity from its neighboring region R_i^1 and R_i^2 is $\sum_{j\in R_i^1} I(j) - \sum_{j\in R_i^2} I(j)$. We can substitute these two components in sign function τ and define $D(i)$ as follows,

$$D(i) = \tau(\sum_{j\in R_i^1} I(j) - \sum_{j\in R_i^2} I(j)). \tag{4}$$

Using (3), (4) can be rewritten as

$$\begin{aligned} D(i) &= \tau(k_d l_d \mathbf{L}(\sum_{j\in R_i^1} \mathbf{n}_j - \sum_{j\in R_i^2} \mathbf{n}_j)) \\ &= \tau(\mathbf{L}(\sum_{j\in R_i^1} \mathbf{n}_j - \sum_{j\in R_i^2} \mathbf{n}_j)). \end{aligned} \tag{5}$$

$D(i)$ is determined by the angle between illumination vector $\mathbf{L}$ and vector $(\sum_{j\in R_i^1} \mathbf{n}_j - \sum_{j\in R_i^2} \mathbf{n}_j)$. For the simplicity, let

$$\begin{aligned} \Delta X_i &= \sum_{j\in R_i^1} x_i - \sum_{j\in R_i^2} x_i, \\ \Delta Y_i &= \sum_{j\in R_i^1} y_i - \sum_{j\in R_i^2} y_i, \\ \Delta Z_i &= \sum_{j\in R_i^1} z_i - \sum_{j\in R_i^2} z_i, \end{aligned} \tag{6}$$

and let $\mathbf{L} = (a, b, c)$, we have

$$D(i) = \tau(\Delta X_i a + \Delta Y_i b + \Delta Z_i c). \tag{7}$$

It may be noted that palmprint images are always acquired under frontal illumination. Therefore, under the Cartesian coordinate in Fig. 1, we have $c > 0$. When $|\Delta Z c_k| > |\Delta X a_k + \Delta Y b_k|$ is satisfied, $D(i)$ is determined by the sign of ΔZ_i, i.e.,

$$\begin{aligned} D(i) &= \tau(\Delta X_i a + \Delta Y_i b + \Delta Z_i c) \\ &= \tau(\Delta Z_i c) = \tau(\Delta Z_i). \end{aligned} \tag{8}$$

According to the description in Sec. 2.1, $\tau(\Delta Z_i)$ represents the DoN feature $DoN(i)$ we plan to recover. (8) illustrates that the 3D information $DoN(i)$ can be recovered from a single 2D image. When constraint $|\Delta Z c_k| > |\Delta X a_k + \Delta Y b_k|$ is satisfied, we can use available texture-level information to recover the 3D shape information.

Without loss of generality, for the sample case when $|\Delta X_i a| > |\Delta Y_i b|$, the constraint can be rewritten as

$$\frac{|c|}{|a|} > \frac{2|\Delta X_i|}{|\Delta Z_i|}. \tag{9}$$

$\frac{|c|}{|a|}$ is determined by the illumination during the imaging which cannot be always controlled. One feasible way to meet the constraint in (9) is to ensure the right side $\frac{2|\Delta X_i|}{|\Delta Z_i|}$ as small as possible. We show that the proper partition for the neighboring regions can be used to achieve this goal which is introduced in next section.

For the simplicity, the partition for each point on the palmprint are set to be the same. Therefore the feature extraction using DoN can be achieved by using a convolution operation followed by a sign function. The partition of the neighboring regions on palmprint images is then replaced by the division of regions on the spatial filter. The spatial regions corresponding to the operating filter is divided into two subsets, say R_1 and R_2 in an $M \times N$ size spatial filter. All the entries in region R_1 are set as 1 and the entries in region R_2 are set as -1. Extending τ to matrix operation, the DoN feature matrix or template $\mathbf{F}$ for image I can be computed as follows:

$$\mathbf{F} = \tau(f * I), \tag{10}$$

(10) is a computationally simpler operation and is used to recover the 3D information from a single 2D image I in our approach.

2.3 Partitioning Local Regions

The second problem outlined in Sec. 2.1 is to decide the neighboring regions. We achieve this goal by partitioning the local regions on the spatial filter as discussed above. Considering the fact that binarized feature template is generated from the (contactless imaging) noisy images, the operator or the filter should be designed in such a way that the positive and negative filtering results from multiple pixels are evened out. This implies that the sum of all the entries in the filter should be zero and the spatial distribution of 1 or -1 in the filter be symmetric and orderly.

On the other hand, as we discussed above, such division should ensure the right side of the constraint in (9) be as small as possible. We now briefly revisit the characteristics of the palmprint surface.

Human palm surface is a complex 3D textured surface consisting of many ridges, wrinkles and lines [3], [4]. The spatial extents of these key elements are different from each other. Generally ridges represent the smallest element while the wrinkles are larger than ridges, and the lines are the most remarkable features in a typical palmprint database. All these key elements share the shape like a valley. The valley typically represents a symmetrical shape whose symmetry axis

is the valley bottom. A 3D palm surface can be seen as a combination of several such symmetrical units. Such units distribute irregularly on palmprint surface. We utilize these properties of such units to make the right side in (9) as small as possible, that is, make ΔX_i approximate to zero and ΔZ_i be a large value.

If the neighboring regions partition is designed to be continuously connected and in patches, it is expected that $\sum_{j\in R_i^1} x_i, \sum_{j\in R_i^2} x_i \approx 0$, thus their difference $\Delta X_i \approx 0$. This is for two reasons: 1) the symmetric units are over x-y plane and such partition ensures the surface symmetry for the regions. When the point normal vectors are added, the azimuth components have large chance to be nearly cancelled out or eliminated (Fig. 2); 2) the x-y plane is almost a *flat* plane, which indicates that the x-component for most of points are excepted to be zero.

The value of ΔZ_i is excepted be large for two reasons, 1) $\sum_{j\in R_i} z_i$ itself is large value since each z_i is a positive value, which is mainly determined by the size and the length of valley; 2) $\sum_{j\in R_i^1} z_i$ is excepted to be different from $\sum_{j\in R_i^2} z_i$ due to the irregular distribution of the valley unit on the palmprint surface.

Therefore, for the palmprint image, $\frac{2|\Delta X_i|}{|\Delta Z_i|}$ is more likely to have small value and satisfy the constraint in (9). Fig. 2 illustrates the summation result of normal vectors from the points on a typical palm line.

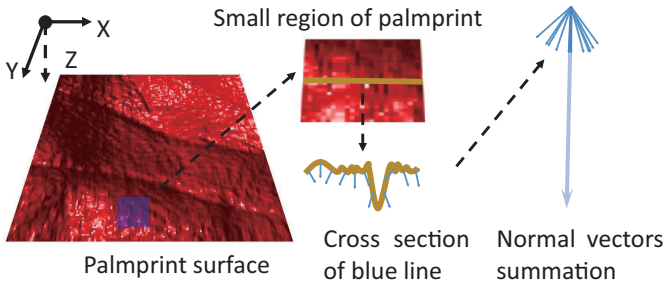

Fig. 2: For a small region on palmprint, if we add the normal vector of each pixel point, the summation result will almost be vertical. This figure illuminates the summation of points on arbitrary palm line.

Fig. 3 illustrates some candidate filters. Fig. 3 (a)-(c) show three such spatial divisions with the *cross* or number of partitions increasing from left to right. Fig. 3 (d)-(f) illustrate spatial distribution of values for the three different directions of a subset when the cross number is fixed to 2. The increase in the number of cross in partitions is expected to help in suppressing the photometric distortions by balancing the filtered results from the positive and negative values. However, too many crosses will make the filter rotationally sensitive. This will also introduce asymmetry by reducing the symmetrical property of the small regions on palmprint, which will make the argument "$\sum_{j\in R_i^1} x_i, \sum_{j\in R_i^2} x_i \approx 0$" unreliable or invalid. Besides, too many crosses will also make "$\Delta Z_i \approx 0$". This can further pose limitations in meeting the constraint in (9).

It may be noted that the symmetrical units (such as ridges, wrinkles and lines) representing dominant palmprint features are expected to have some width. The direction of intersection

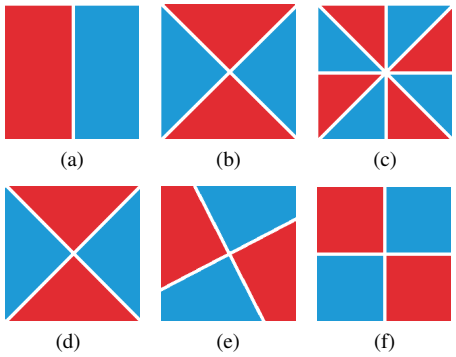

Fig. 3: Different colors represent different subsets in a filter. In (a)-(c) the crossing in the filter increases from 1 to 3 while in (d)-(f) the directions of filters are varied when the crossing is fixed to 2.

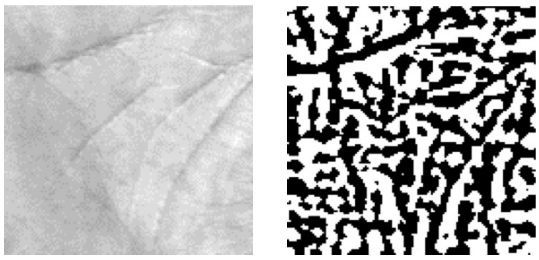

Fig. 4: The feature code of palmprint. (a) Original gray level image. (b) The feature code.

boundary (center or white line on filter in Fig. 3) also has width. In order to ensure the symmetry, the white line in the filter configuration should be located orthogonal or parallel to the dominant symmetrical units. The experimental results in Sec. 4.2 also support these arguments.

According to previous analysis, the filter of Fig. 3 (b) is selected to construct the feature extractor or the filter. This filter can be defined as follows:

$$f_{i,j} = \begin{cases} 1 & |i| > |j| \\ -1 & |i| < |j| \\ 0 & otherwise. \end{cases} \tag{11}$$

where i, j is the indexes,$i, j \in [-B, B]$. The filter size is $(2B+1) \times (2B+1)$. Fig. 4 shows a typical palmprint ROI image and its encoded features.

2.4 Template Denoising and Matching

Our analysis in previous sections suggests that the constraint in (9) may not be satisfied for some cases. This can be due to two key reasons: 1) in some of the extreme locations, there is still a chance that $\Delta Z_i \approx 0$, and 2) when portion of the valleys appears on the boundary or edges of the filter, the response from the small regions will no longer be symmetrical.

In order to alleviate the unreliable codes or features resulting from the noise or extreme cases as discussed above, we incorporate a denoising strategy during matching. The morphological operations, i.e., opening operation and closing operation, are performed on the feature templates, and the weighted sum of three scores is computed as the final matching score. The morphological operations are adopted for two reasons, 1) the noisy perturbations due to the limitations of the feature extractor are expected to be discretely distributed

in the feature templates and 2) the feature template is binary and has spatial continuity. It should be noted that this step does not increase the feature template size.

Given two feature template $\mathbf{F}_1$ and $\mathbf{F}_2$, the matching distance is computed by the weighted sum of three scores,

$$dis(\mathbf{F}_1, \mathbf{F}_2) = w_1 S(\mathbf{F}_1, \mathbf{F}_2) + w_2 S(\widetilde{\mathbf{F}}_\mathbf{1}, \widetilde{\mathbf{F}}_\mathbf{2}) + w_3 S(\widehat{\mathbf{F}}_\mathbf{1}, \widehat{\mathbf{F}}_\mathbf{2}), \tag{12}$$

where $\widetilde{\mathbf{F}}$ and $\widehat{\mathbf{F}}$ are the results after applying closing and opening operations on feature template $\mathbf{F}$. $S(\mathbf{F}_1, \mathbf{F}_2)$ is defined as

$$S(\mathbf{F}_1, \mathbf{F}_2) = \frac{\Gamma(\mathbf{F}_1 \otimes \mathbf{F}_2 \& M(\mathbf{F}_1) \& M(\mathbf{F}_2))}{\Gamma(M(I_1) \& M(I_2))}, \tag{13}$$

where $\otimes$ and $\&$ are XOR and AND operation, $\Gamma(\mathbf{F})$ computes the number of non-zero value in matrix $\mathbf{F}$, $M(I)$ is the mask matrix indicating the valid region on palmprint image I. It is define as

$$M(I)(i,j) = \begin{cases} 0, & background \\ 1, & otherwise. \end{cases} \tag{14}$$

We use horizontal and vertical translations between two matched templates to improve alignment. In all our experiments, the best match score among these alignments is used as the final match score.

3 Analysis on Palmprint Matching

The DoN feature for each point on the image can have only two values. Therefore, it is necessary to analysis whether this feature can be powerful enough for the accurate palmprint matching. The DoN feature is a kind of ordinal measure. In the literature, Sinha [5] believed that ordinal measure can only be used for simple detection or classification task and it should be impossible using ordinal measure alone to solve complex object recognition problems. This concern arises from the nature of ordinal measure which loses some numerical information. Sun *et al.* [6], [7] demonstrated that the ordinal measure can play a defining role for the complex iris recognition and palmprint recognition problems. They achieved significant performance improvement over competing methods. However, they essentially used *three* features to increase the discrimination of the ordinal measure and the discrimination using only one feature based on ordinal measure was not investigated. Besides, they achieved most of the success from designing the feature extractor, i.e., using derivation of Gaussian filter, and did not provide much analysis for the role played by the ordinal measure. In this section, we demonstrate that a single feature based on ordinal measure can be very powerful for the palmprint matching.

In the palmprint matching, feature or template of a palmprint image is usually a feature matrix [6], [8], [9], [10], [11], [12]. Each entry on the matrix is an encoded feature code. Distance between two templates is defined as the sum of distances between such codes. Hamming distance is usually employed to measure the codes' distance as the codes are often binarized. In ordinal measure, the number of encoding classes for each code is 2 while in CompCode [9] or RLOC [8], the encoding classes is 6. For simplicity, the number of encoding classes is represented by λ in the following analysis.

Let us consider the similarity between two palmprint templates being matched. If these two palmprint images belong to the same subject, we refer them as intra-class matching distance or genuine matching distance. Similarly, if these templates belong to different subjects, we refer them as inter-class matching distance or imposter matching distance. In order to simplify the analysis, distance between two codes is assumed to be zero if they are equal, otherwise one. For a 128×128 palmprint template, the dimension of its feature vector is 16384. Considering the spatial dependence of palmprint region, it is quite reasonable to assume that the intrinsic dimension of a single palmprint feature vector, let us denote here by M, is much smaller than 16384, i.e., $M \ll 16384$. For the convenience of illustrations, we can consider a certain value for M, say 1000.

Considering the inter-class matching attempts, whether the codes on the templates are matched or mismatched can be considered as a random event. This is because two palmprints are from different subjects and are unknown. Therefore, we assume [2] that the distribution of inter-class matching distance D_{inter} follows Binomial distribution

$$D_{inter} \sim B(n_{inter}, p), \tag{15}$$

where n_{inter} is the number of trials in the Binomial distribution which is the same as M, p is the success probability. The relation between λ and p can be expressed as

$$p = 1 - \frac{1}{\lambda}. \tag{16}$$

Fig. 5 (a) shows the inter-class distance distributions when $n_{iter} = 1000$, λ is 6 and 2 respectively. This figure illustrates the inter-class palmprint matching scores for the ideal cases, i.e., when features are robust and free from imaging variations, with the changes in λ.

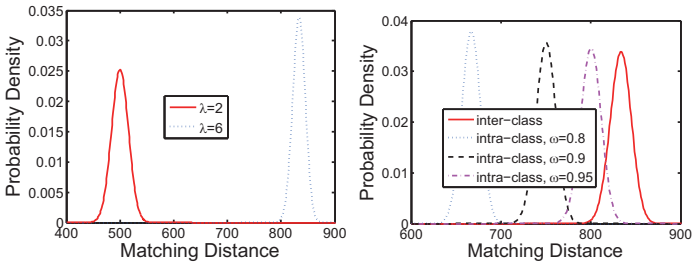

(a) (b)

Fig. 5: (a) Typical matching distance distribution for different λ. (b) When $p = \frac{5}{6}$, the inter-class distance distribution and three intra-class distance distribution with different ω.

Considering the intra-class matching attempts, among all the codes pairs, we call the codes pair as reliable when both of participating matching codes are encoded in the right class[3], otherwise the pairs are considered as unreliable. For a reliable codes pair, the matching distance should certainly be zero. For an unreliable pair, the matching distance still have chance to be

2. Analysis of iris codes using millions of matching scores presented by Daugman [13] also justifies this assumption.

3. Right class describes the actual depth information.

zero. Therefore, the intra-class matching distance between two templates is effectively determined by the number of unreliable codes pairs. For the unreliable pairs, whether these respective codes are matched or not can also be considered as a random event. This is because the unreliable codes are mainly caused by noise and misalignment whose exact influence unknown. Representing the number of unreliable pairs as ωM, where ω is the unreliable pairs rate $(0 < \omega < 1)$, we assume intra-class matching distance D_{intra} follows the Binomial distribution

$$D_{intra} \sim B(n_{intra}, p), \tag{17}$$

n_{intra} is number of trials, which is equal to the unreliable pairs number ωM, p is the success probability. The relationship between p and λ is the same as for inter-class distance distribution. When $\lambda = 6, M = 1000$, several intra-class distance distributions with different ω as well as the inter-class distance distribution are shown in Fig. 5 (b). From this figure, we can observe that when ω becomes larger, which means the number of unreliable pairs is large, the overlapping area between intra-class and inter-class distance distributions also becomes larger. It is known that in order to achieve accurate identification, least overlap between the intra-class and inter-class matching distance distribution is desirable.

The likelihood of an unreliable pair being generated can be estimated as

$$\theta = 1 - (1 - p)(1 - p). \tag{18}$$

It may be noted that the ω also represents the expected rate of unreliable code pairs. Therefore it is quite reasonable to assume that ω is proportional to θ, i.e.,

$$\omega \propto \theta. \tag{19}$$

Given two λ, the relation between their corresponding p_i, p_2, ω_1, and ω_2 can be expressed as

$$\frac{\omega_1}{\omega_2} = \frac{1 - (1 - p_1)(1 - p_1)}{1 - (1 - p_2)(1 - p_2)}. \tag{20}$$

When two λ are 6 and 2, p_1 is $\frac{5}{6}$ and p_2 is $\frac{1}{2}$ respectively, given $\omega_1 = 0.95, 0.98$, according to (20), the corresponding $\omega_2 = 0.73, 0.76$. Fig. 6 (a) and (b) show these distribution with $\omega_1 = 0.95, 0.98$ respectively.

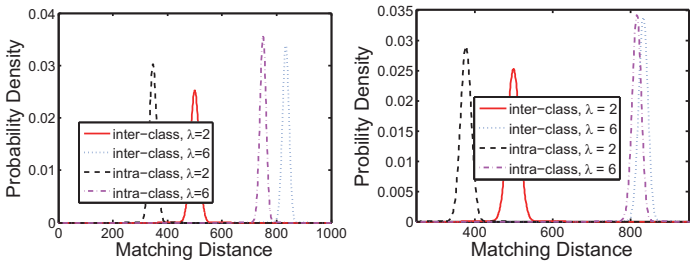

(a) (b)

Fig. 6: (a) If $\omega_1 = 0.95$, the inter-class and intra-class distance distribution with λ = 2 and λ = 6 respectively. (b) If $\omega_1 = 0.98$, the inter-class and intra-class distance distribution with λ = 2 and λ = 6 respectively.

We can observe from Fig. 6 that under the same condition, the overlapping area between inter-class and intra-class distance distributions for $\lambda = 2$ is always smaller than that for $\lambda = 6$. No overlap means the inter-class distance is always larger than intra-class distance, which results in good performance. Note that $\lambda = 2$ means the feature template is binary, it is expected that binary representation for feature is more effective.

The analysis presented in this section theoretically argues the effectiveness of ordinal measure for palmprint matching. This argument is further supported by our experimental results on 2D palmprint databases in Sec. 4.4.

4 Experimental Validation and Results

In this section, we firstly evaluate the performance from our method on four publicly available 2D palmprint databases. Three competing methods, RLOC [8], CompCode [9], and Ordinal Code [6] are implemented[4] for the comparative performance. To facilitate fair comparison with prior work, different protocols are adopted for different databases. The computation complexity is also compared.

In order provide detailed analysis on our method, the performance from our method using different filters (Fig. 3) as well as without denoising strategy is also reported. To demonstrate the robustness of our feature to the illumination changes, the experiment from a face database with significant illumination changes is also reported. Besides, a fast version of CompCode, namely Fast-CompCode, which is based on the ordinal measure, is employed to support the arguments we made in Sec. 3.

4.1 Experimental Results from Proposed Method

4.1.1 PolyU Contactless 2D/3D Palmprint Database

This contactless palmprint database [15] is acquired from 177 different subjects (right hand). There are 20 samples from each subject with 10 2D images and 10 depth images. It also provides segmented palmprint images of 128×128 pixels. Our experiments are performed on full 2D part of this database. The 2D images in this database are acquired under poor (ambient) illumination conditions.

In our experiment, the first 5 samples of each subject are enrolled as training set. The rest 5 are as the test set. There are 885 samples for training/gallery and 885 samples for testing/probe. The ROC, CMC curves as well as the EER are used to evaluate the performance.

The poor or ambient illumination in this database, along with contactless imaging, makes it most challenging among other databases. Fig. 7 illustrates the ROC and CMC curves. Table 1 provides the EER and average rank-one recognition accuracy. It can be observed that the proposed method achieves outperforming results over the other methods for both the verification and identification.

4.1.2 IITD Palmprint Database

The IITD touchless palmprint database [16] provides contactless palmprint images from the right and left hands of 230 subjects. There are more than 5 samples for each right hand or left hand. This database provides 150×150 pixels segmented palmprint images.

4. The three methods are implemented by us. All of the results using the version of our implementation achieve similar or slightly better than those reported in the authors' paper [8], [9], [14], with same protocol and same datasets. The implementation as well as the parameters can be found on [1].

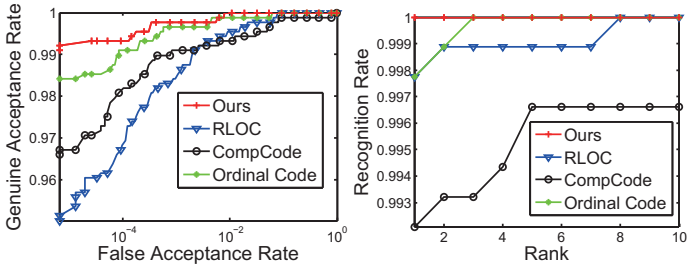

(a) (b)

Fig. 7: (a) The ROC curves and (b) CMC curves of different methods from the PolyU 2D/3D contactless palmprint database.

TABLE 1: The EER and rank-one recognition rate (accuracy) of different methods from PolyU 2D/3D palmprint database.

Method	Ours	RLOC	Competitive Code	Ordinal Code
EER (%)	**0.22**	0.64	0.68	0.33
Accuracy (%)	**100**	99.77	99.21	99.77

The protocol is exactly the same as in [10]. All the 1300 right hand palmprint images are used for our experiments. For each subject, one image for testing and the rest for training. The average performance is reported. The ROC, EER and CMC are used to ascertain the performance. Fig. 8 illustrates the ROC and CMC curves. Table 2 presents the EER and average rank-one recognition accuracy. The EER and rank-one recognition rate from our method achieves outperforming results.

TABLE 2: The EER and rank-one recognition rate (accuracy) of different methods from the IITD palmprint database.

Method	Ours	RLOC	Competitive Code	Ordinal Code
EER (%)	**0.68**	0.88	1.0	1.25
Accuracy (%)	**99.15**	99.00	98.85	98.92

4.1.3 PolyU Palmprint Database

The PolyU palmprint database [17] contains 7752 palmprint images from 386 different palms. These images were automatically segmented to 128×128 pixel. In this database, there are several images which are poorly aligned due to their rotational variation. In our experiments, we used the same protocol as reported in [8]. Only the first sample of each individual is used to construct the training set. Then, the training set is enlarged by rotating each image in training set at -9°, -6°, -3°, 3°, 6° and 9° respectively. Consequently, there are seven training samples for each of the palms from database.

Fig. 9 illustrates the comparative ROC and CMC curves. Table 3 summarizes the EER and rank-one recognition accuracy from different methods. The results from our method and the Ordinal Code are superior than those from the other two methods.

Note that the performance from our method is observed to be slightly better than that of Ordinal Code. The reason for the performance improvement not being significant, for this PolyU palmprint database, is that the Ordinal Code is special case of our feature. This palmprint database is a contact-based database acquired under controlled or very good illumination condition. The direction of illumination vector $\mathbf{L}$ is almost parallel to z-axis (Fig. 1). In this case, the left side

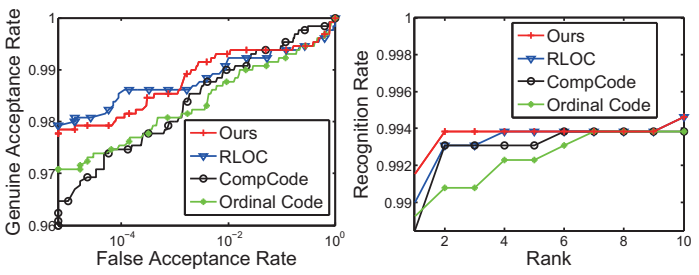

(a) (b)

Fig. 8: (a) The ROC curves and (b) CMC curves of different methods from the IITD palmprint database.

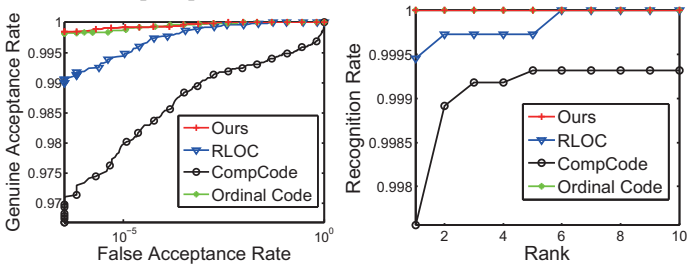

(a) (b)

Fig. 9: (a) The ROC curves and (b) CMC curves of different methods from the PolyU palmprint database.

of the constraint in (9) is large enough to make it is satisfied. According to our previous analysis, the Ordinal Code method is essentially the difference between the weighted combination of the point normal vectors. Even if the filter is not carefully designed, the constraint in (9) is excepted to hold good. Note that the feature size of Ordinal Code is *three* times larger than ours, while our method outperforms Ordinal Code.

TABLE 3: The EER and rank-one recognition rate (accuracy) of different methods from PolyU palmprint database.

Method	Ours	RLOC	Competitive Code	Ordinal Code
EER (%)	**0.033**	0.089	0.076	0.038
Accuracy (%)	**100**	99.95	99.76	100

4.1.4 CASIA Palmprint Database

The CASIA palmprint database contains 5239 palmprint images from 301 individuals. It is the largest publicly available palmprint database in terms of the number of individuals.

In this database, the individual "101" is the same as the individual "19" and therefore these two classes were merged into one class. The 11th image from the left hand of individual "270" is also misplaced to the right hand. The 3rd image from left hand of individual "76" is a distorted sample whose quality is very poor. These two samples can also be automatically detected by our palmprint segmentation program [1]. We eliminated these two images in our experiment. Therefore all our experiments with this database used 5237 images belonging to 600 different palms. We segmented and scaled the resulting images in the database to 128×128 pixels. In our experiments, the total number of resulting matches is 13,692,466, which includes 20,567 genuine and 13,689,899 imposter matches.

Fig. 10 illustrates the ROC and CMC results from the proposed method, RLOC, competitive code and Ordinal Code.

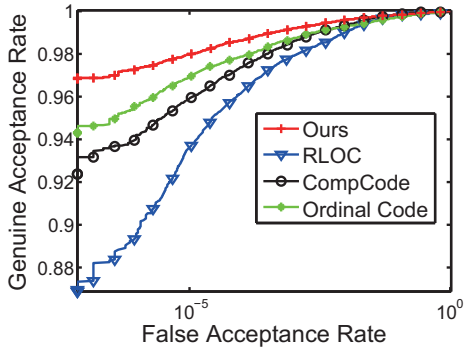

Fig. 10: The ROC curves from the CASIA palmprint database.

Table 4 summarizes EER achieved from these methods. Our method significantly outperforms competing three methods.

TABLE 4: The EER(%) comparison from CASIA palmprint database.

Method	Ours	RLOC	Competitive Code	Ordinal Code
EER	**0.53**	1.0	0.76	0.79

4.1.5 Computational Complexity

Table 5 lists the computational time for our method, RLOC, CompCode and Ordinal Code. The matching speed of our method is the fastest among other methods. The feature extraction speed of our method is much faster than the CompCode, Ordinal Code and marginally slower than for RLOC. However, the matching speed of our method is more than 22 times faster than that for the RLOC.

TABLE 5: Feature extraction and matching time (ms) of different methods.

Method	Feature Extraction	Matching
Ours	1.1	**0.054**
RLOC	**0.13**	1.2
Competitive Code	4.0	0.054
Ordinal Code	3.2	0.054

Note: The experimental environment is: Windows 8 Professional, Intel(R) Core(TM) i5-3210M CPU@2.50GHz, 8G RAM, VS 2010.

4.2 Additional Experimental Results

In this section, we investigate the influence of using different filter configurations as well as the denoising strategy for the palmprint matching performance. We use four publicly available databases employed in earlier experiments, with their described protocols, to ascertain the performance from other filter configurations. The weight ratio and filter size have been empirically selected to achieve the illustrated performance.

The EER results using the different filter configurations in Fig. 3 are shown in Fig. 11. The experimental results validate our analysis presented in Sec. 2.3, regarding the expected influence in the performance from the variations in the number of cross and the directions of the different subset. The filter we selected achieves the best performance as illustrated. The results for the three competing methods are also shown in the figure. All the other filter results are also not significantly inferior because they are ordinal measures and they can still extract robust codes or feature in their respective templates.

This figure also illustrates the results without using the denoising strategy, i.e., employing $dis(\mathbf{F}_1, \mathbf{F}_2) = S(\mathbf{F}_1, \mathbf{F}_2)$. instead of (12), to compute the matching distance. As can be observed from the results, even without employing the denoising strategy, our feature can also achieve competing performance with the state-of-the-art methods reported in the literature. It should be noted that without denoising strategy, the matching speed is **three times faster**.

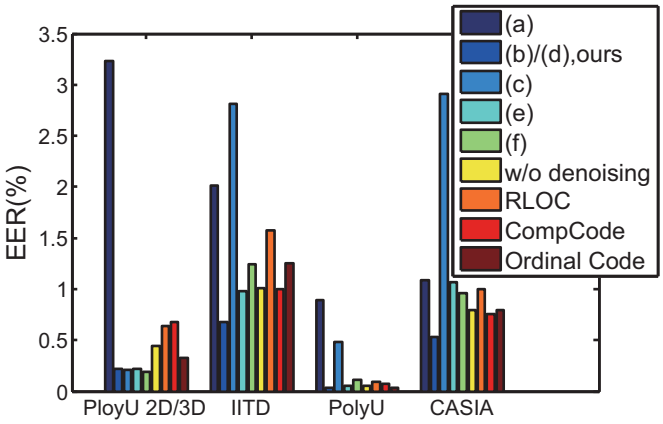

Fig. 11: Comparative performance using EER from different filter configurations for four palmprint databases.

4.3 Experiment on Yale Face Database

In this experiment, Extended Yale Face Database B [18] is employed. These experiments are not intended to investigate our feature on face surface, but we just want to evaluate the effectiveness of our feature to support the arguments that our feature is indeed describing the 3D shape information which is insensitive to illumination changes. We choose Extended Yale Face Database B to achieve the goal for three reasons:

1) There are only few palmprint images acquired under extreme lighting conditions. The face data, whose surface is almost flat, is similar to palmprint surface.
2) This database is acquired under extreme illumination variations.
3) The face data in this database doesn't have any view or expression variations.

The Extended Yale Face Database B contains 38 subjects and each subject is with 64 illumination conditions. The cropped faces with the resolution of 168×192 are also provided. In our experiment, the most neutral light sources (A+000E+00) images are used as the gallery, and all the other frontal images are used as probes (in summary, 38 images constitute the training set and 2376 images as test set). This database is used to evaluate the identification performance.

We do not design additional filters according to the geometrical properties of the face surface but simply use the same division strategy as for the palmprint. Besides, the denoising matching strategy is not employed to underline our feature's robustness to the extremely varying illumination conditions.

The rank-one recognition result is 99.3% which is the state-of-the-art performance. Table 6 provides the comparison with another two state-of-art methods on this database. The results demonstrate that our feature is also robust to the illumination variations.

TABLE 6: Identification rate comparison with the state-of-the-art methods from the Extended Yale Face Database B.

Method	Ours	PP+LTP/DT [19]	G_LDP [20]
Rank-1 rate (%)	**99.3**	99.0	97.9

4.4 Experimental Results from Fast-CompCode

The experiments in this section are used to verify the effectiveness of ordinal measure for the 2D palmprint matching. Firstly, we simplify the CompCode to generate binary representation feature.

As reported in [9], the CompCode uses six filters to generate six pre-templates. In the simplified version, two of the six filters (the orientation of these two filters are orthogonal) are used to generate two intermediate pre-templates and subsequently binary template is generated as the final feature. The rest of implementation of the CompCode is the same as in [9]. This method is referred [21] to as Fast-CompCode.

Fig. 12 illustrates the ROC for the Fast-CompCode and CompCode on four 2D palmprint databases using the same protocols as reported above. It can be observed that the performance of simplified/ordinal approach is superior to that of original one. Therefore it is reasonable to conclude that ordinal measure is not only faster but also more accurate which validates our analysis in Sec. 3.

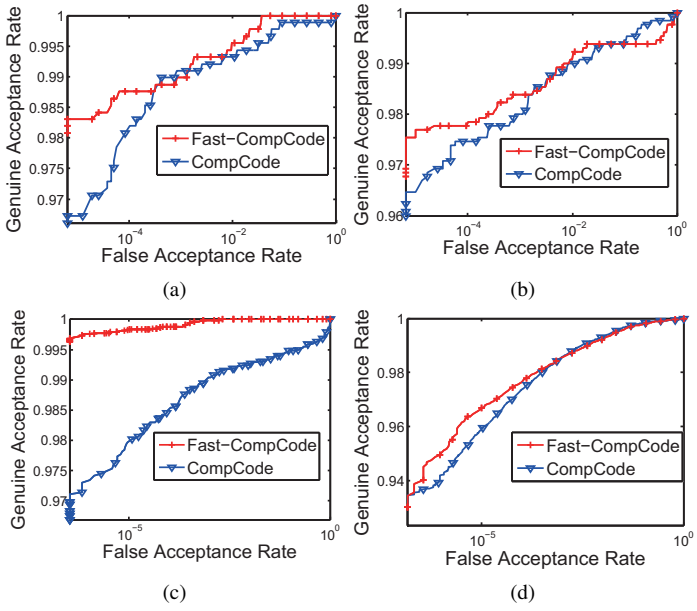

Fig. 12: The ROC curves for Fast-CompCode and CompCode from (a) PolyU Contactless 2D/3D database, (b) IITD palmprint database, (c) PolyU 2D palmprint database and (d) CASIA 2D palmprint database.

5 Conclusions

This paper has proposed a new feature which is based on ordinal measure. This feature recovers 3D shape information of the surface while it is extracted from pixel level information in the contactless images. The feature extraction and matching is very efficient and the implementation is simple which emphasizes on its practicality. The template size from this feature is also very small while it achieves excellent performances on many databases.

The proposed feature is suitable to be combined [3] with other features to further improve the performance. There are two key reasons: 1) it has lower storage requirements while being efficient to recover/extract and match, and most importantly it is effective in achieving accurate performance, 2) most of 2D feature mentioned in previous sections extract the texture information while our feature is recovering 3D shape information, which means it is likely to have less redundancy than the other features.

Despite promising results, there are several aspects of proposed approach that require further consideration. The impact of non-Lambertian surface and non-linear palm deformations, in the feature recovery and matching, requires further study and analysis.

References

[1] Weblink for downloading codes for *all* algorithms in this paper, available from: http://www4.comp.polyu.edu.hk/~csajaykr/2Dto3D.htm.

[2] R. Basri and D. W. Jacobs, "Lambertian reflectance and linear subspaces," *Patt. Anal. Mach. Intell., IEEE Trans. on*, vol. 25, no. 2, pp. 218–233, 2003.

[3] A. Kumar and C. Kwong, "Towards contactless, low-cost and accurate 3d fingerprint identification," *Pattern Analysis and Machine Intelligence, IEEE Transactions on*, vol. 37, no. 3, pp. 681–696, 2015.

[4] D. Maltoni, D. Maio, A. K. Jain, and S. Prabhakar, *Handbook of fingerprint recognition*. Springer Science & Business Media, 2009.

[5] P. Sinha, "Qualitative representations for recognition," in *Biologically Motivated Computer Vision*. Springer, 2002, pp. 249–262.

[6] Z. Sun, T. Tan, Y. Wang, and S. Z. Li, "Ordinal palmprint represention for personal identification [represention read representation]," in *Comp. Vis. Patt. Recogn., 2005. CVPR 2005. IEEE Computer Society Conf. on*, vol. 1. IEEE, 2005, pp. 279–284.

[7] Z. Sun and T. Tan, "Ordinal measures for iris recognition," *Patt. Anal. Mach. Intell., IEEE Trans. on*, vol. 31, no. 12, pp. 2211–2226, 2009.

[8] W. Jia, D.-S. Huang, and D. Zhang, "Palmprint verification based on robust line orientation code," *Patt. Recogn.*, pp. 1504–1513, 2008.

[9] A.-K. Kong and D. Zhang, "Competitive coding scheme for palmprint verification," in *Patt. Recogn., 2004. ICPR 2004. Proc. of the 17th Inter. Conf. on*, vol. 1. IEEE, 2004, pp. 520–523.

[10] A. Kumar and S. Shekhar, "Personal identification using multibiometrics rank-level fusion," *Systems, Man, and Cybernetics, Part C: Applications and Reviews, IEEE Trans. on*, vol. 41, no. 5, pp. 743–752, 2011.

[11] V. Kanhangad, A. Kumar, and D. Zhang, "A unified framework for contactless hand verification," *Info. Fore. Sec., IEEE Trans. on*, vol. 6, no. 3, pp. 1014–1027, 2011.

[12] D. Zhang, W.-K. Kong, J. You, and M. Wong, "Online palmprint identification," *Patt. Anal. Mach. Intell., IEEE Trans. on*, vol. 25, no. 9, pp. 1041–1050, 2003.

[13] J. Daugman, "The importance of being random: statistical principles of iris recognition," *Patt. recogn.*, vol. 36, no. 2, pp. 279–291, 2003.

[14] D. N. Bhat and S. K. Nayar, "Ordinal measures for image correspondence," *Patt. Anal. Mach. Intell., IEEE Trans. on*, vol. 20, no. 4, pp. 415–423, 1998.

[15] "The Hong Kong Polytechnic University Contact-free 3D/2D Hand Images Database (Ver 1.0)," available online.

[16] "IIT Delhi Touchless Palmprint Database (Ver 1.0). (2015, Jun. 10). [online]," available from: http://web.iitd.ac.in/~ajaykr/Database_Palm.htm.

[17] "PolyU Palmprint Palmprint Database [online]," The Hong Kong Polytechnic University, http://www.comp.polyu.edu.hk/~biometrics/.

[18] K.-C. Lee, J. Ho, and D. J. Kriegman, "Acquiring linear subspaces for face recognition under variable lighting," *Patt. Anal. Mach. Intell., IEEE Trans. on*, vol. 27, no. 5, pp. 684–698, 2005.

[19] X. Tan and B. Triggs, "Enhanced local texture feature sets for face recognition under difficult lighting conditions," *Image Proc., IEEE Trans. on*, vol. 19, no. 6, pp. 1635–1650, 2010.

[20] B. Zhang, Y. Gao, S. Zhao, and J. Liu, "Local derivative pattern versus local binary pattern: face recognition with high-order local pattern descriptor," *Image Proc., IEEE Trans. on*, vol. 19, pp. 533–544, 2010.

[21] Q. Zheng, A. Kumar, and G. Pan, "Suspecting less and achieving more: new insights on palmprint identification for faster and more accurate matching," *Info. Fore. Sec., IEEE Trans. on*, 2015.